Molecular modeling and nonlinear optical properties of new isostructural halogenated dihydroquinolinones

Loide O. Sallum[1,2], Clodoaldo Valverde[1,2], Igor L. Andrade[1], Giulio D. C. D'Oliveira[3], Caridad. N. Perez[3], Ademir. J. Camargo[1], Francisco A. P. Osório[4,5], Tertius L. Fonseca[4] and H. B. Napolitano[1,2]**

[1] Grupo de Química Teórica e Estrutural de Anápolis, Universidade Estadual de Goiás, 75001-970, Anápolis, GO, Brazil.
[2] Laboratório de Novos Materiais, Universidade Evangélica de Goiás, Anápolis, GO, Brazil.
[3] Laboratório de Modelagem Molecular Aplicada e Simulação, Universidade Paulista, 74845-090, Goiânia, GO, Brazil.
[4] Instituto de Química, Universidade Federal de Goiás, 74690-970, Goiânia, GO, Brazil.
[5] Instituto de Física, Universidade Federal de Goiás, 74.690-900, Goiânia, GO, Brazil.
[6] Pontifícia Universidade Católica de Goiás, 13566-590, Goiânia, GO, Brazil.

* Corresponding authors: Clodoaldo Valverde (valverde@ueg.br); H. B. Napolitano (hamilton@ueg.br)

Abstract

Two new isostructural halogenated dihydroquinolinones were synthesized and characterized by single crystal X-ray diffraction. A detailed isostructural analysis of the electronic and optical properties is presented using density functional theory models with emphasis on structure-property relationship in the solid phase. The physical-chemical properties such as molecular electrostatic potential, frontier molecular orbitals as well as nature of intermolecular interactions and interaction energy of dimeric structures are almost unaffected by the replacement of the bromine atom by the chlorine atom. Starting from the embedded unit cells, the third-order nonlinear susceptibility ($\chi^{(3)}$) of the newly synthesized crystals has been estimated by using an iterative electrostatic scheme, in which the surrounding molecules are represented by point charges. Theoretical results illustrate the role played by the environment polarization effect and halogenated substituents on $\chi^{(3)}$. which has the same order of magnitude as those observed in other organic crystals. Our findings suggest that the dihydroquinolinone derivative crystals are very promising NLO materials.

Keywords: *isostructural dihydroquinolinones; X-ray diffraction; M06-2X/6-311++G(d,p); NLO properties.*

Table S1. Angles and dihedral angles (º) representation for BMP and CMP.

BMP			
O2-S1-O3	119.68(1)	C24-S1-N1-C1	-86.69
O3-S1-N1	106.71(1)	C24-S1-N1-C9	54.54
C1-N1-C9	113.68(1)	C2-C10-C11-C12	-34.40
N1-C9-C8	120.90(1)	C1-C2-C10-C11	-9.76
S1-C24-C29	119.22(1)	C2-C10-C11-C16	151.86
O2-S1-N1	106.71(1)	C3-C2-C10-C11	174.58
O3-S1-C24	109.18(1)	S1-N1-C1-C17	-148.39
S1-N1-C1	119.59(1)	C17-C1-C2-C3	-86.76
N1-C1-C2	109.90(1)	N1-C1-C17-C22	68.15
O2-S1-C24	107.68(1)	C9-N1-C1-C17	69.79
N1-S1-C24	106.10(1)	N1-C1-C17-C18	-109.29
S1-N1-C9	115.32(1)	C1-N1-C9-C8	-140.38
N1-C1-C17	105.98(1)	C3-C4-C9-C8	-178.49
S1-C24-C25	119.46(1)	C5-C4-C9-N1	179.70
CMP			
O2-S1-O3	119.58(1)	C24-S1-N1-C1	86.79
O3-S1-N1	106.74(1)	C24-S1-N1-C9	-54.47
C1-N1-C9	113.41(1)	C2-C10-C11-C12	33.95
N1-C9-C8	120.78(1)	C1-C2-C10-C11	9.71
S1-C24-C29	119.20(1)	C2-C10-C11-C16	-152.02
O2-S1-N1	106.85(1)	C3-C2-C10-C11	-174.80
O3-S1-C24	109.19(1)	S1-N1-C1-C17	148.43
S1-N1-C1	119.71(1)	C17-C1-C2-C3	86.65
N1-C1-C2	109.82(1)	N1-C1-C17-C22	-69.13
O2-S1-C24	107.66(1)	C9-N1-C1-C17	-69.53
N1-S1-C24	106.06(1)	N1-C1-C17-C18	107.58
S1-N1-C9	115.56(1)	C1-N1-C9-C8	140.01
N1-C1-C17	106.02(1)	C3-C4-C9-C8	178.74
S1-C24-C25	119.22(1)	C5-C4-C9-N1	-179.89

Table S2. The major intermolecular interactions NBO analysis using DFT wavefunctions for BMP and CMP.

Donor (i)	Acceptor (j)	E(2)[a]	E(j) – E(i)[b,c]	F(i,j)[b,d]
BMP				
LP[e] (1) Br1	BD*(2) C19 – C20	0.11	1.12	0.011
BD(2) C19 – C20	BD*(1) Br1	0.47	0.43	0.014
BD*[f](2) C19 – C20	BD*(1) Br1	0.42	0.07	0.011
LP (1) O1	BD*(1) C7 – H7	0.16	1.56	0.014
LP (2) O1	BD*(1) C7 – H7	0.32	1.14	0.017
LP (1) O2	BD*(1) C28 – H28	0.24	1.74	0.018
LP (3) O2	BD*(1) C28 – H28	0.11	1.16	0.010
BD*(1) S1 – O2	BD*(1) C28 – H28	0.12	0.51	0.027
LP (1) O3	BD*(1) C26 – H26	0.20	1.75	0.017
LP (3) O3	BD*(1) C26 – H26	0.20	1.17	0.014
BD*(1) S1 – O3	BD*(1) C26 – H26	0.10	0.53	0.025
BD(1) C26 – H26	BD*(1) S1 – O3	0.06	0.89	0.007
LP (3) O3	BD*(1) C16 – H16	0.29	1.16	0.017
LP (3) O2	BD*(1) C16 – H16	0.07	1.15	0.008
CMP				
LP[e] (1) Cl1	BD*(2) C19 – C20	0.07	1.09	0.008
BD(2) C19 – C20	BD*(1) Cl1	0.23	0.46	0.010
BD*[f](2) C19 – C20	BD*(1) Cl1	0.16	0.10	0.008
LP (1) O1	BD*(1) C7 – H7	0.16	1.56	0.014
LP (2) O1	BD*(1) C7 – H7	0.32	1.14	0.017
LP (1) O2	BD*(1) C28 – H28	0.26	1.74	0.019
LP (3) O2	BD*(1) C28 – H28	0.11	1.16	0.010
BD*(1) S1 – O2	BD*(1) C28 – H28	0.13	0.51	0.028
LP (1) O3	BD*(1) C26 – H26	0.21	1.75	0.017
LP (3) O3	BD*(1) C26 – H26	0.20	1.17	0.014
BD*(1) S1 – O3	BD*(1) C26 – H26	0.10	0.53	0.025
BD(1) C26 – H26	BD*(1) S1 – O3	0.06	0.89	0.007
LP (3) O3	BD*(1) C16 – H16	0.28	1.16	0.017
LP (3) O2	BD*(1) C16 – H16	0.06	1.15	0.008

(a) kcal/mol; (b) atomic units; (c) Energy difference between donor and acceptor i and j NBO orbitals; (d) F(i,j) is the Fock matrix element between i and j NBO orbitals; (e) LP(n)A is a valence lone pair orbital (n) on A atom; (f) (*) denotes antibonding.

Table S3. DFT results for refractive index of the isolated and embedded molecules of BMP and CMP obtained using the 6311++G(d,p) basis set.

	M11*		CAM-B3LYP	
	Isolated	Embedded	Isolated	Embedded
BMP				
static	1.71	1.71	1.69	1.69
532nm	1.80	1.80	1.77	1.77
CMP				
static	1.69	1.69	1.67	1.67
532nm	1.77	1.77	1.75	1.75

The refractive index of the embedded BMP structure (wavelength = 532 nm) was calculated using the functional CAM-B3LYP [Equation (S1)]:

$$\frac{n(\omega)^2 - 1}{n(\omega)^2 + 2} = \frac{4\pi Z}{3V}\langle\alpha(-\omega;\omega)\rangle. \tag{S1}$$

where $Z = 8$, $V = 4825.0$ Å^3 and $\langle\alpha(-\omega;\omega)\rangle = 60.05 \times 10^{-24} esu$ (1 esu = 1 cm^3 and 1 Å^3 = 10^{-24} cm^3). The refractive index n is equal to 1.77.

Table S4. DFT results for third-order nonlinear susceptibility ($\chi^{(3)}$), in $10^{-22}m^2/V^2$, of the BMP and CMP crystals obtained using the 6311++G(d,p) basis set ($\chi^{(3)}$ in esu = 7.1619x $10^7\chi^{(3)}$ $in\ m^2/V^2$).

	M11*		CAM-B3LYP	
	Isolated	Embedded	Isolated	Embedded
BMP				
static	137.87	144.79	124.4	126.10
532nm	619.45	692.54	480.49	521.00
CMP				
static	80.11	129.45	102.08	101.28
532nm	419.39	558.15	376.38	398.29

The nonlinear third-order susceptibility of the BMP (wavelength = 532 nm) was calculated using the functional CAM-B3LYP [(Equations (S2 and S3)]:

$$\chi^{(3)}(-\omega;\omega,\omega,-\omega) = f^4\frac{Z}{V}\langle\gamma(-\omega;\omega,\omega,-\omega)\rangle. \tag{S2}$$

$$f = \frac{(n(\omega)^2+2)}{3}. \tag{S3}$$

The average second hyperpolarizability, associated with the nonlinear optical process of the intensity-dependent refractive index (IDRI), was calculated using the Equation (S4):

$$\langle\gamma(-\omega;\omega,\omega,-\omega)\rangle \cong 2\langle\gamma(-\omega;\omega,0,0)\rangle - \langle\gamma(0;0,0,0)\rangle. \tag{S4}$$

where $\langle\gamma(-\omega;\omega,0,0)\rangle = 169.65x10^{-36}esu$ and $\langle\gamma(0;0,0,0)\rangle = 79.41x10^{-36}esu$, that $\langle\gamma(-\omega;\omega,\omega,-\omega)\rangle = 259.89x10^{-36}esu$. The following values were considered in the calculation of the $\chi^{(3)}$: Z = 8, V = 4825.0 Å³ and $\langle\gamma(-\omega;\omega,\omega,-\omega)\rangle = 259.89 \times 10^{-36}esu$ [$1\gamma\left(\frac{m^5}{V^2}\right) = \frac{4\pi}{9} \times 10^{-14}\gamma(esu)$, 1Å³ = 10⁻³⁰ m³ and $n(\omega)$ = 1.77]. The $\chi^{(3)}(-\omega;\omega,\omega,-\omega)\ is\ equal\ to\ 521 \times 10^{-22}\frac{m^2}{V^2}$.

HOMO (-178.62 kcal/mol)　　　　　LUMO (-42.91 kcal/mol)

(a)

HOMO (-178.78 kcal/mol)　　　　　LUMO (-42.47 kcal/mol)
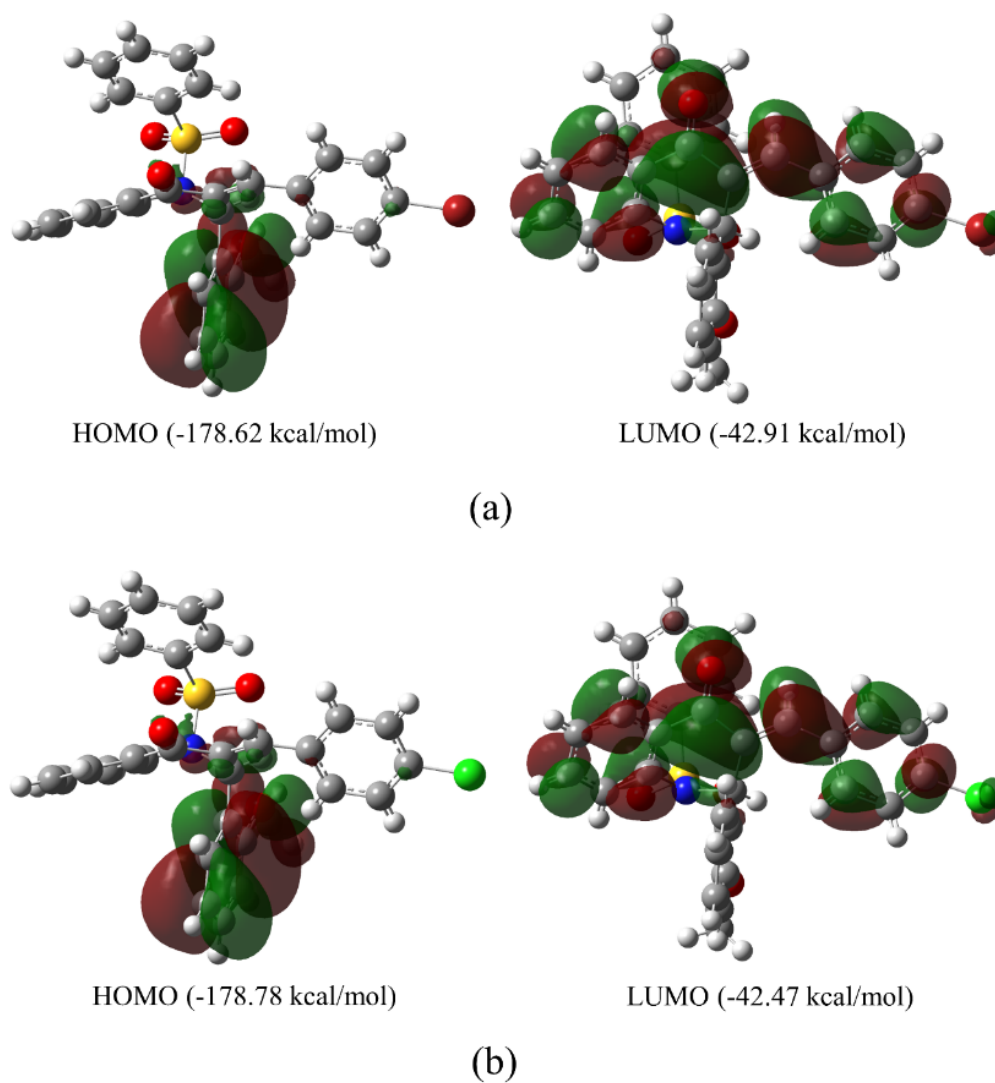
(b)

Figure S1. Frontier molecular orbitals derived from Khon-Sham analysis at M06-2X/6-311++G(d,p) level of theory with the isovalue of 0.02 atomic units: the HOMO π-bonding orbital and the LUMO π-antibonding orbital for (a) BMP and (b) CMP.
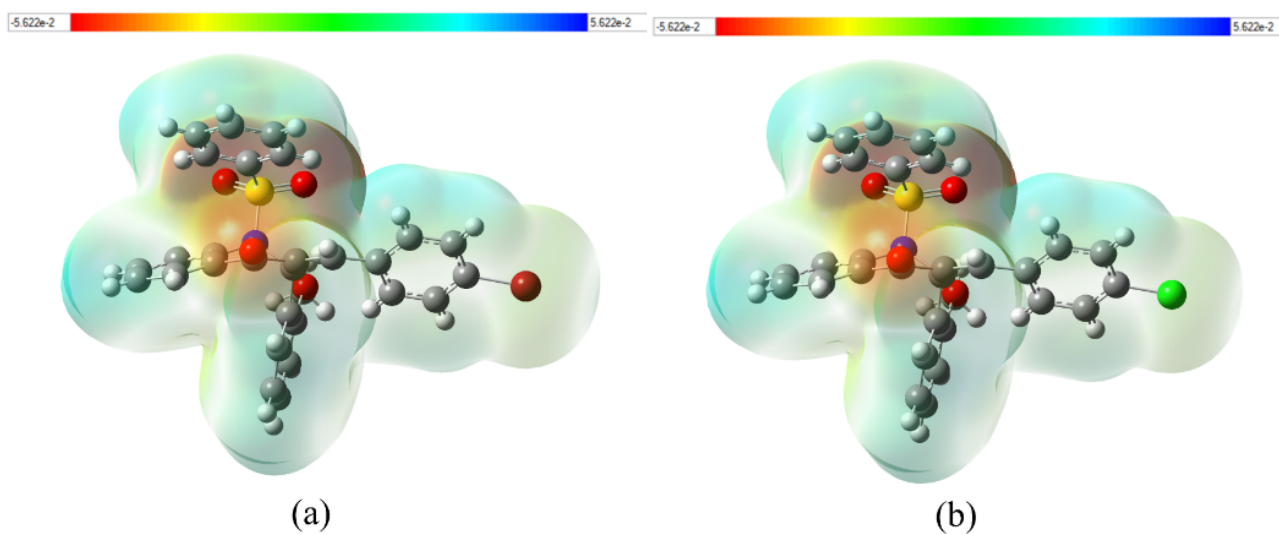
Figure S2. The molecular electrostatic potential surface mapped for (a) BMP and (b) CMP shows the red-colored region rich in electrons, and the blue-colored region, which is electron depleted. The density value of 4.0 x 10^{-4} electrons/bohr^3 was used to generate the molecular electrostatic potential surfaces.
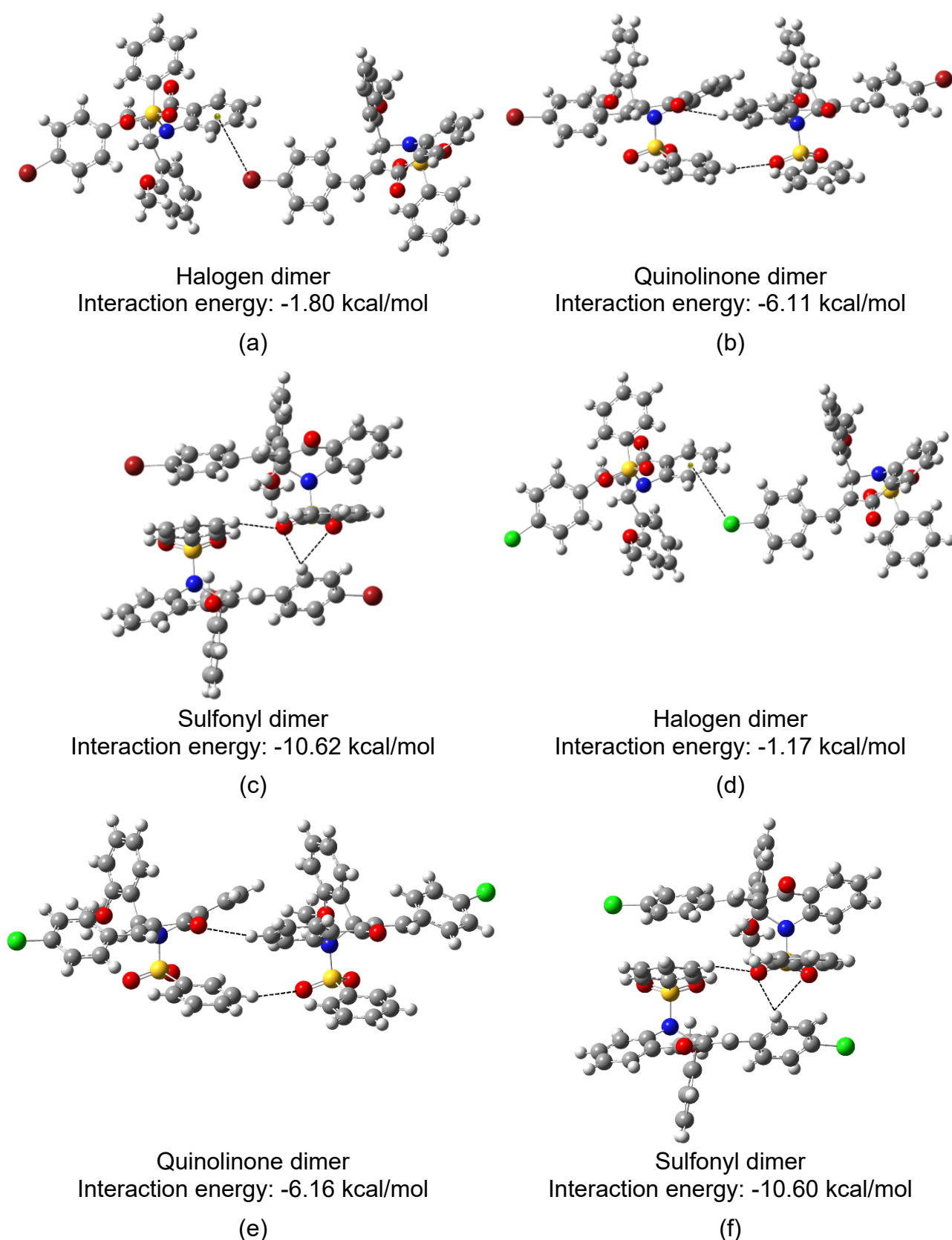
Halogen dimer
Interaction energy: -1.80 kcal/mol

(a)

Quinolinone dimer
Interaction energy: -6.11 kcal/mol

(b)

Sulfonyl dimer
Interaction energy: -10.62 kcal/mol

(c)

Halogen dimer
Interaction energy: -1.17 kcal/mol

(d)

Quinolinone dimer
Interaction energy: -6.16 kcal/mol

(e)

Sulfonyl dimer
Interaction energy: -10.60 kcal/mol

(f)

Figure S3. Complexation energies obtained at M06-2X/6-311++G(d,p) level of theory: side-to-side dimers respectively (a) $C_{14}-Br_1\cdots\pi$, (b) $C_7-H_7\cdots O_1$, $C_{28}-H_{28}\cdots O_2$ and (c) $C_{26}-H_{26}\cdots O_3$, $C_{16}-H_{16}\cdots O_3$ and $C_{16}-H_{16}\cdots O_2$ for BMP; (d) $C_{14}-Cl_1\cdots\pi$, (e) $C_7-H_7\cdots O_1$, $C_{28}-H_{28}\cdots O_2$ and (f) $C_{26}-H_{26}\cdots O_3$, $C_{16}-H_{16}\cdots O_3$ and $C_{16}-H_{16}\cdots O_2$ for CMP.
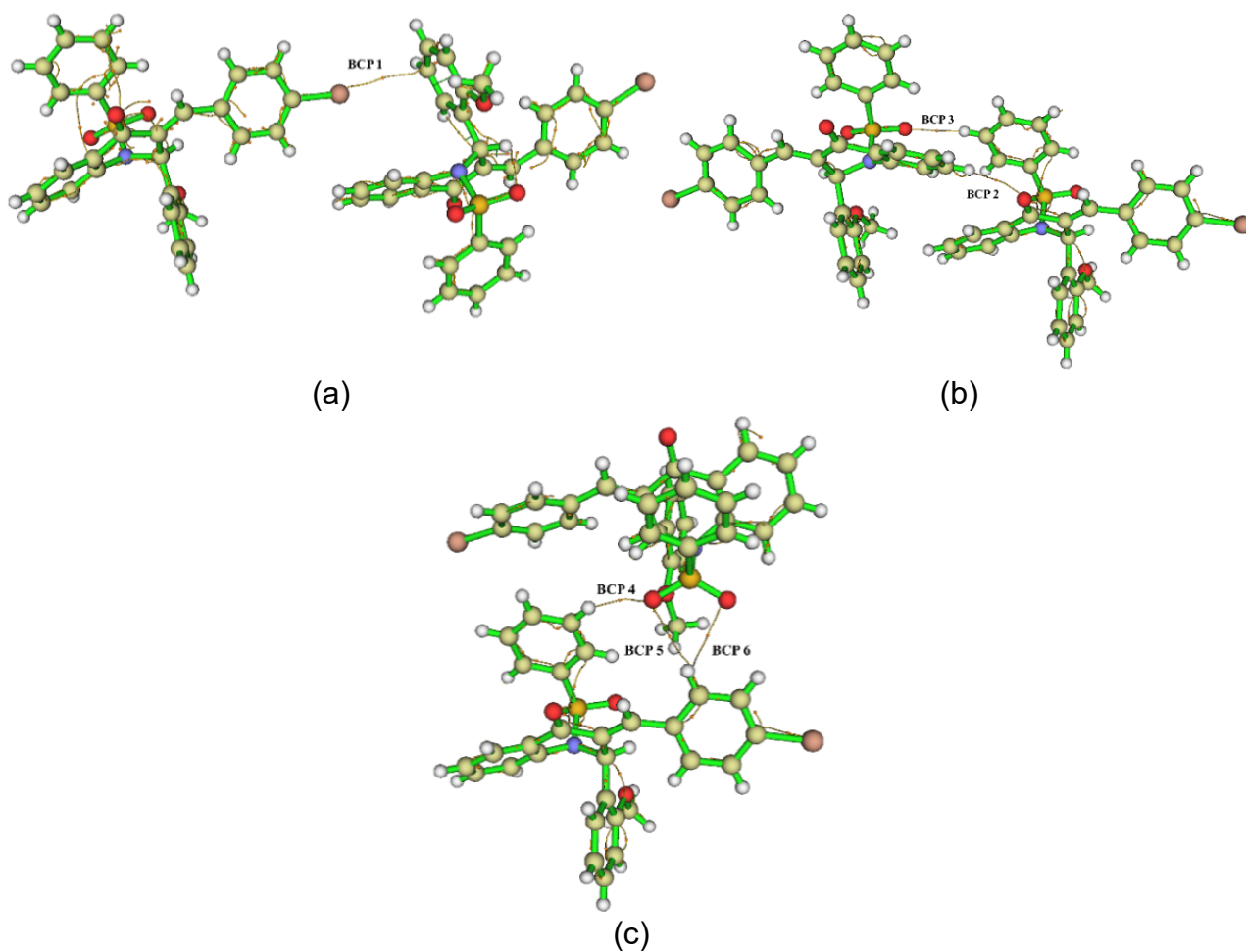
(a)

(b)

(c)

Figure S4. The molecular graph of dimers' interactions respectively: (a) C_{14}–$Br_1 \cdots \pi$, (b) C_7–$H_7 \cdots O_1$, C_{28}–$H_{28} \cdots O_2$ and (c) C_{26}–$H_{26} \cdots O_3$, C_{16}–$H_{16} \cdots O_3$ and C_{16}–$H_{16} \cdots O_2$ for BMP, showing the bond critical points (BCPs) in yellow.
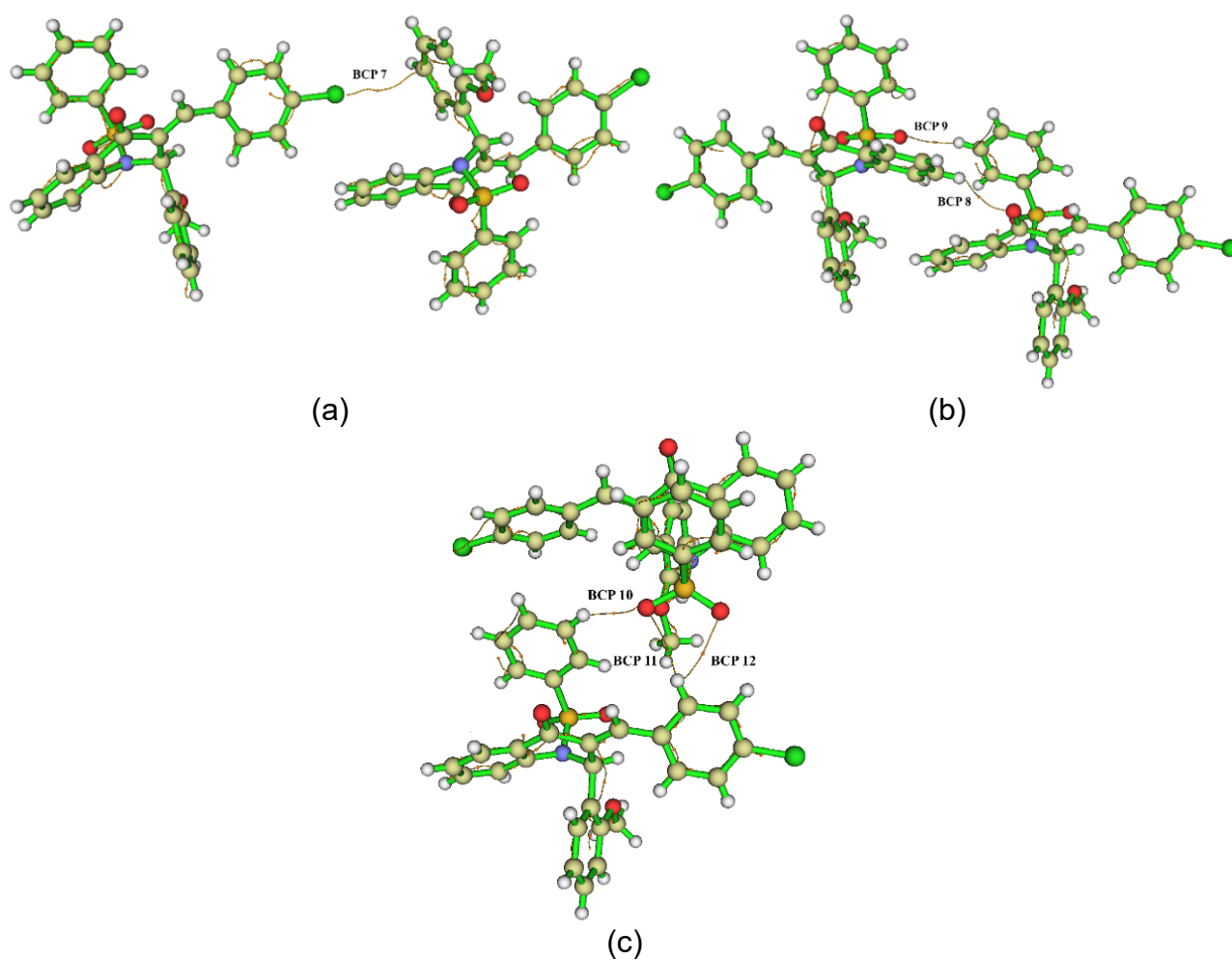
Figure S5. The molecular graph of dimer interactions respectively: (a) C_{14}–Cl_1···π, (b) C_7–H_7···O_1, C_{28}–H_{28}···O_2 and (c) C_{26}–H_{26}···O_3, C_{16}–H_{16}···O_3 and C_{16}–H_{16}···O_2 for CMP, showing the bond critical points (BCPs) in yellow.

BMP

CMP

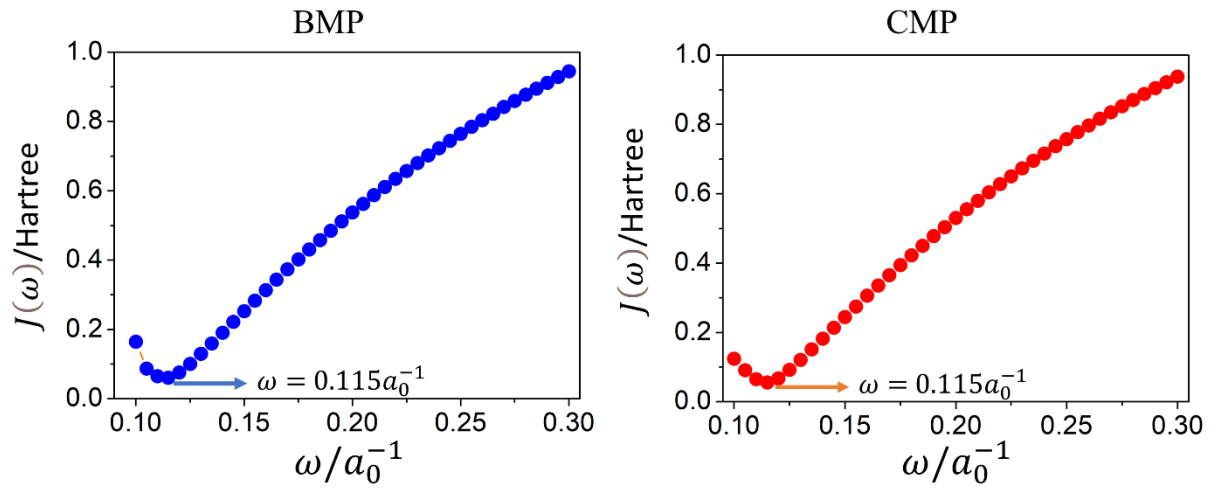$\omega = 0.115a_0^{-1}$

$\omega = 0.115a_0^{-1}$

Figure S6. The range separation parameter $\varpi = \omega/a_0^{-1}$ is then adjusted in an iterative procedure such that $J(\varpi) = J(\omega)/\text{Hartree}$ is minimized.